

# MORPHOLOGIC DESCRIPTION OF THE PUNTA COLA ROCK AVALANCHE AND ASSOCIATED MINOR ROCKSLIDES CAUSED BY THE 21 APRIL 2007 AYSÉN EARTHQUAKE (PATAGONIA, SOUTHERN CHILE)

Thierry OPPIKOFER<sup>1\*</sup>, Reginald L. HERMANN<sup>1</sup>, Tim F. REDFIELD<sup>1</sup>, Sergio A. SEPÚLVEDA<sup>2</sup>, Paul DUHART<sup>3</sup> and Ignacio BASCUÑÁN<sup>3</sup>

<sup>1</sup>International Centre of Geohazards, Geological Survey of Norway, Postboks 6315 Sluppen, 7491 Trondheim, Norway

<sup>2</sup>Departamento de Geología, Universidad de Chile, Santiago, Chile

<sup>3</sup>Servicio Nacional de Geología y Minería de Chile, Puerto Varas, Chile

\*Corresponding author: Thierry Oppikofer, thierry.oppikofer@ngu.no

## ABSTRACT

The 21 April 2007 Aysén earthquake triggered hundreds of landslides in the epicentral area, including several large-volume rock avalanches that caused tsunamis in the Aysén fjord. This study is part of a larger project aiming to better understand the conditioning factors controlling size and distribution of earthquake-triggered landslides. The focus is set on the largest rockslide that occurred at Punta Cola. Using a high-resolution digital surface model created from terrestrial laser scanning, a detailed geomorphologic map of the rockslide scars and the rock avalanche deposits on land was made. This map permitted to establish the sequence of events: the failure of the rockslide main compartment led to a rock avalanche that crossed the valley and ran up on the opposite valley flank before turning downstream and impacting the fjord and creating a tsunami. Afterwards, another rockslide compartment failed and piled up 80 m thick deposits in the valley. Seven minor rockslides occurred in the Punta Cola valley after the main rock avalanche. The volumes of rockslides and associated deposits were estimated using the sloping local base level technique that allows computing the possible pre-rockslide topography and the bedrock-deposits interface. These volume computations give 22.4 Mm<sup>3</sup> for the Punta Cola rockslide, which is significantly more than previous estimates (12 Mm<sup>3</sup>). The on-shore deposits of the main rock avalanche have a volume of 13.7 Mm<sup>3</sup> and approximately 14.4 Mm<sup>3</sup> are deposited in the fjord. This study highlights the additional information on rockslides and rock avalanches that can be obtained from high-resolution 3D data and mapping.

**Keywords:** *terrestrial laser scanning; digital elevation model; scar; deposits; volume computation*

## RESUMEN

*Descripción morfológica de la avalancha de rocas de Punta Cola y deslizamientos de rocas asociados causados por el terremoto de Aysén del 21 de abril de 2007 (Patagonia, sur de Chile).*

El terremoto de Aysén del 21 de abril de 2007 generó cientos de remociones en masa en la zona epicentral, incluyendo varias avalanchas de roca de gran volumen que causaron tsunamis en el fiordo Aysén. Este estudio es parte de un proyecto orientado a una mejor comprensión de los factores que controlan el tamaño y distribución de remociones en masa generadas por sismos. El estudio se centra en el deslizamiento de mayor tamaño, ocurrido en el sector de Punta Cola. Mediante el uso de un modelo de terreno digital de alta resolución creado a partir de un escaneo láser terrestre, se preparó un mapa geomorfológico de las zonas de arranque y depósitos de la avalancha de roca, el cual permite establecer la secuencia de eventos: la falla de la sección mayor de deslizamiento derivó a una avalancha de roca que cruzó el valle trepando el flanco opuesto antes de girar hacia aguas abajo e impactar el fiordo generando un tsunami. Posteriormente, otra parte de la ladera falló generando un depósito de hasta 80 m de espesor en el valle. Siete deslizamientos menores ocurrieron a lo largo del valle después de la avalancha principal. Los volúmenes de los deslizamientos y depósitos asociados fueron estimados usando la técnica de nivel base local, la cual permite estimar la topografía pre-deslizamiento y el contacto entre los depósitos y el sustrato rocoso. Se calculó un volumen de 22,4 Mm<sup>3</sup> para el deslizamiento de Punta Cola, notoriamente mayor que estimaciones previas (12 Mm<sup>3</sup>). Los depósitos en tierra de la avalancha tienen un volumen de 13,7 Mm<sup>3</sup> mientras aproximadamente 14,4 Mm<sup>3</sup> se habrían depositado en el fiordo. Este estudio resalta la información adicional sobre deslizamientos y avalanchas de roca que puede obtenerse a partir de mapeo 3D de alta resolución.

**Palabras clave:** *Escaneo láser terrestre; modelo de elevación digital; zona de arranque; depósitos; cálculo de volumen*

## INTRODUCTION

Large rockslides and rock avalanches are a major natural hazard in many mountainous areas (Evans and Clague 1994) and have continuously occurred throughout the Andes (Hermannns *et al.* 2008). Their consequences in terms of infrastructure damage and life losses can be catastrophic, especially when they impact water bodies and create devastating tsunamis. Fjords are particularly prone for tsunamigenic rockslides, due to the steep mountainsides flanking the fjord. This hazard can be increased in seismically active areas, such as the Chilean coast.

On 21 April 2007 the Aysén fjord earthquake ( $M_w$  6.2) in southern Chilean Patagonia triggered 538 landslides in the epicentral area along the fjord coast and surroundings (Sepúlveda and Serey 2009;

Sepúlveda *et al.* 2010) (Fig. 1). The seismicity was associated with tectonic activity in the Liquiñe-Ofqui Fault Zone (LOFZ), a major structural feature of the region. The landslides included rockslides and rock avalanches, rockfalls, shallow soil and soil-rock slides, and debris flows (Sepúlveda *et al.* 2010). Some of the major rockslides and rock avalanches caused large tsunami waves that impacted the fjord coasts.

Our project aims to understand the condition factors controlling size and distribution of earthquake-triggered landslides. This includes detailed structural analysis of fault zones in the Aysén fjord region, on-site engineering geological and structural mapping, terrestrial laser scanning (TLS) and photogrammetric analysis of selected rockslide sites, as well as the elaboration of detailed digital elevation models (DEMs) before and after the 2007 earthquake.

This study focuses on the geomorphologic analysis of the Punta Cola rock avalanche (Fig. 1) based on high-resolution digital surface model (HR-DSM) provided by TLS. A detailed geomorphologic map combining the HR-DSM and field observations is presented and used to establish a sequence of events that occurred during and after the 2007 Aysén earthquake. The volumes of rockslides and rock avalanche deposits are also assessed using the sloping local base level (SLBL) algorithm (Jaboyedoff *et al.* 2004).

## Terrestrial laser scanning for landslide investigation

Terrestrial laser scanning (TLS) is a novel technique for landslide investigations and monitoring (Jaboyedoff *et al.* 2012). The high-resolution topography data provided by TLS are useful for mapping and characterization of landslides (Rowlands *et al.* 2003; Dunning *et al.* 2009; Jaboyedoff *et al.* 2009a). One of the major uses of TLS on rockfalls and rockslides is the characterisation of main structures, including their orientation (Abellán *et al.* 2006; Kemeny *et al.* 2006; Jaboyedoff *et al.* 2007; Lato *et al.* 2009; Oppikofer *et al.* 2009; Sturzenegger and Stead 2009b), spacing and persistence (Kemeny *et al.* 2006; Sturzenegger and Stead 2009b), or surface roughness (Fardin *et al.* 2001; Kulatilake *et al.* 2006; Sturzenegger and Stead 2009a; Oppikofer *et al.* 2011). This is particularly useful for inaccessible, remote or hazardous rock walls.

In landslide susceptibility and hazard assessment, TLS is useful for the creation of high-resolution DEMs for site-specific slope stability modelling (e.g. Jaboyedoff *et al.* 2009b) and run-out modelling (Alba *et al.* 2005; Nguyen *et al.* 2011), especially when precise topographic information is not available from other sources (e.g. airborne laser scanning DEM). Multi-temporal TLS point clouds provide crucial input for rockfall hazard assessment by enabling the localisation of rockfall activity and the quantification of rockfall volumes and mechanisms (Rosser *et al.* 2005; Abellán *et al.* 2006; Abellán *et al.* 2010; Pedrazzini *et al.* 2010).

Landslide displacements can be efficiently

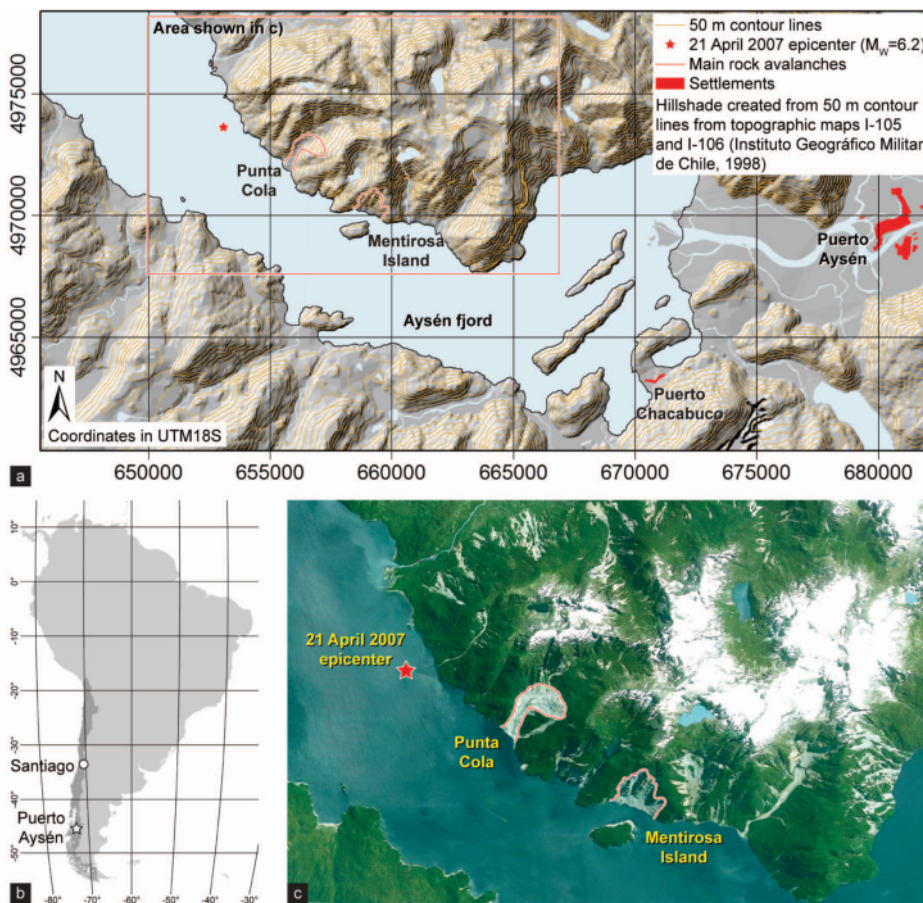


**Figure 1:** Maps of the study area: a) Hillshade map; b) Location map of the Aysén fjord in southern Chile; c) Orthophoto of the epicentral area of the 2007 Aysén earthquake and the main earthquake-triggered rock avalanches of Punta Cola and Mentirosa Island. Epicentre location based on Legrand *et al.* (2011).

monitored by multi-temporal TLS acquisitions. In opposition to conventional, point-based surveying techniques (GPS, total station etc.), TLS is an area-based technique and provides information over the entire landslide area. This enables a more complete understanding of the landslide displacements (Bitelli *et al.* 2004; Teza *et al.* 2007; Oppikofer *et al.* 2008; Jaboyedoff *et al.* 2009a; Oppikofer *et al.* 2009; Abellán *et al.* 2010).

## SITE DESCRIPTION

### 21 April 2007 Aysén earthquake

The EW to NW-SE-trending Aysén fjord is a typical glacial valley with a U-shape and steep flanks. The fjord is located within the dioritic to granitic North Patagonian Batholith of Mesozoic to Early Cenozoic age that intruded into the metamorphic Paleozoic basement and the Mesozoic metasedimentary and metavolcanic units (e.g. Pankhurst *et al.* 1999). The fjord is crossed by the LOFZ, which has been identified as the main neotectonic-seismotectonic feature of Patagonia (e.g. Cembrano *et al.* 1996; 2002). This more than 1000 km-long, NNE-trending, nearly vertical, dextral strike-slip fault is related to the oblique subduction of the Nazca Plate under the South American Plate and accommodates the parallel component of the convergent deformation (e.g. Lavenu and Cembrano, 1999; Cembrano *et al.* 2002). The LOFZ also appears to control the location of Quaternary volcanoes (e.g. Cembrano *et al.* 1996) and a series of earthquakes and seismic swarms along the LOFZ indicates a reactivation of movement along the fault (Naranjo *et al.* 2009). Further North along the fault zone, a cluster of 19 rock slope failures with a volume of up to 4 km<sup>3</sup> is directly related to the spatial distribution of fault segments (Folguera *et al.* 2004; Hermanns *et al.* 2011; Penna *et al.* 2011). In the Aysén fjord this reactivation has manifested itself as a seismic swarm that began on 22 January 2007 and that climaxed in the 21 April 2007 Aysén earthquake. This earthquake had a magnitude Mw of 6.2 and had an intensity of VII on

the modified Mercalli scale in the towns of Puerto Aysén and Puerto Chacabuco, located 25 km and 20 km from the epicentre, respectively (Naranjo *et al.* 2009; Sepúlveda *et al.* 2010) (Fig. 1a).

The 21 April 2007 Aysén earthquake triggered 538 landslides in the epicentral area (up to 42 km away) (Sepúlveda *et al.* 2010), including 282 soil-rock slides, 135 soil slides, but also 34 rockslides and rock avalanches. Most events occurred on the northern flank of the fjord and its lateral valleys. Two large rockslides and rock avalanches occurred in front of Mentirosa Island and in the Punta Cola creek with estimated volumes of 8 and 12 Mm<sup>3</sup>, respectively (Sepúlveda and Serey 2009; Sepúlveda *et al.* 2010) (Fig. 1a,c). Both rock avalanches caused tsunamis in the fjord, which impacted the coast line, destroyed some houses and several salmon farms in the fjord. Ten persons lost their life by landslides and associated tsunamis triggered by the 21 April 2007 Aysén earthquake (Naranjo *et al.* 2009; Sepúlveda and Serey 2009; Sepúlveda *et al.* 2010).

### Punta Cola rock avalanche

The Punta Cola rockslide and rock avalanche was the largest landslide triggered by the 21 April 2007 Aysén earthquake (Sepúlveda and Serey 2009; Sepúlveda *et al.* 2010). The rockslide scar is located on a NW-dipping slope in a lateral valley of the Aysén fjord at a distance of 1 to 1.5 km from the shoreline (Fig. 1a, Fig. 2). After the initial failure, the rockslide transformed into a rock avalanche that ran down the narrow valley, impacted the fjord and triggered one of the tsunamis in the Aysén fjord. The rock avalanche had a very high mobility with a maximum run-up height of more than 150 m on the opposite valley flank (Redfield *et al.* 2011) (Fig. 2b, d). The rock avalanche caused significant erosion in the valley and its flanks, leading to entrainment of soil, rock and vegetation (Sepúlveda and Serey 2009; Sepúlveda *et al.* 2010). Several secondary landslides occurred along the valley flanks and were probably triggered by scouring of the valley flanks by the Punta Cola rock avalanche and/or by earthquake aftershocks (Sepúlveda *et al.* 2010; Redfield *et al.* 2011) (Fig. 2b, d).

## METHODS

### Terrestrial laser scanning technique

Terrestrial laser scanning (TLS) is based on the reflectorless and contactless acquisition of a point cloud of the topography using the time-of-flight distance measurement of an infrared laser pulse (Baltsavias 1999; Lichti *et al.* 2002): 1. A monochromatic and highly collimated laser pulse is emitted by the scanner in a precisely known direction determined by a horizontal and a vertical angle relative to the scanner axis; 2. The laser pulse gets back-scattered by the surface (terrain, vegetation, buildings etc.) and the return signal is recorded by the scanner; 3. Using the time-of-flight of the pulse, the distance between the scanner and the object is computed; 4. The 3D coordinates of the recorded point relative to the scanner are known by its distance and its directional angles; 5. A point cloud is obtained by sweeping the laser pulse in different directions, using for example rotating mirrors inside the instrument.

The Optech ILRIS-3D ER used for this study has a wavelength of 1500 nm and a range in practice of about 800 to 1200 m on rock slopes, depending on the reflectivity of the object (Optech 2011). The manufacturer specifies a point accuracy of 7 mm on the range and 8 mm on the position at a distance of 100 m. The Optech ILRIS-3D ER scans with a frequency of 2500 points per second and can cover a 40° wide and 40° high field of view in a single acquisition. The angular spacing between two laser pulses is user-defined and enables the creation of high-resolution point clouds (minimum: 2 mm at a distance of 100 m). In practice, the chosen point spacing ranges from 1 to 15 cm, depending on the distance between the scanner and the object and the scope of the study.

### TLS data acquisition and treatment

The Punta Cola rock avalanche scar and deposits were scanned between 25 and 30 January 2010. In order to cover as completely as possible the study area, a total of 58 scans were acquired from 11 viewpoints on the rock avalanche deposits (Fig. 3). The scans have a mean point

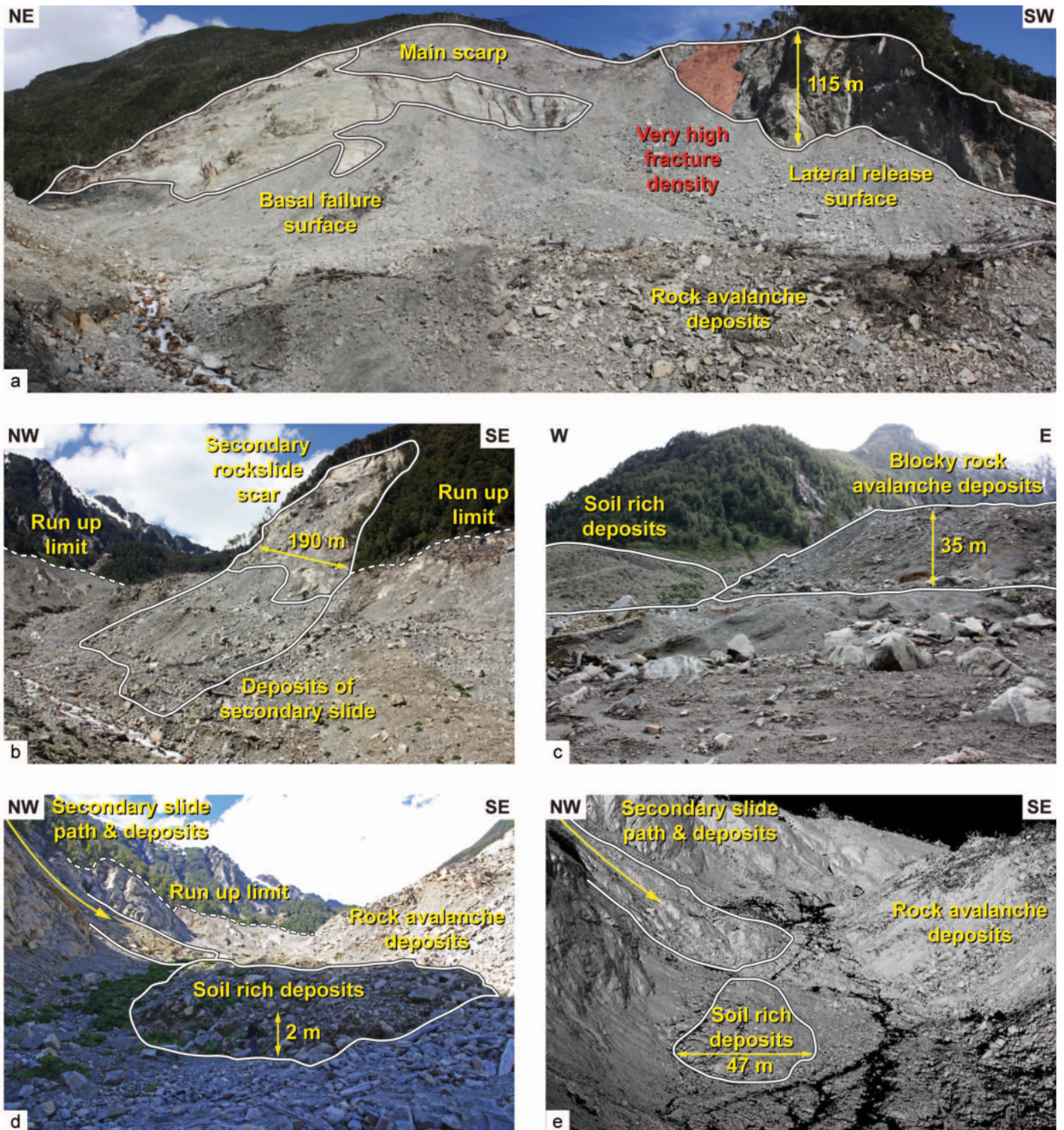


**Figure 2:** Photographs of the Punta Cola rock avalanche: a) panorama of the rockslide scar displaying the outcropping basal failure surface and the 115 m high lateral release surface. A branch of the LOFZ passes across the lateral release surface and the head scarp; b) secondary rockslide scar, associated deposits and run up limits of the main rock avalanche on the right valley side; c) steep rock avalanche deposits with different compositions (blocky vs. soil rich); d) lobate soil rich landslide deposits in the run out area of the Punta Cola rock avalanche attest that scouring by the rock avalanche along valley flanks caused secondary landslides contributing significantly to the total landslide volume; e) terrestrial laser scanner point cloud with similar view as the photograph reveals the morphology of the different deposits, including the soil rich lobe deposited onto the main rock avalanche deposits.

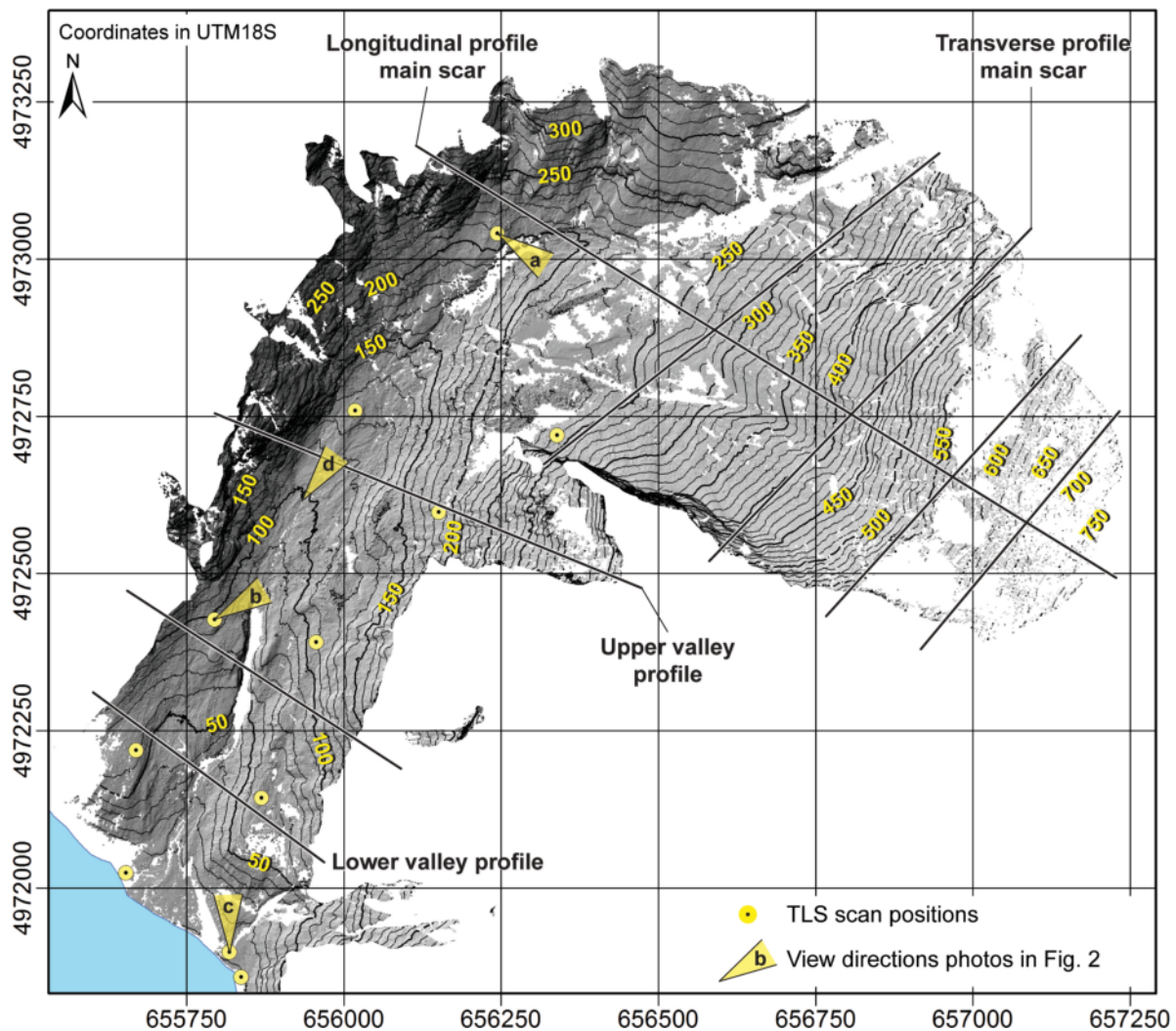


**Figure 3:** Hillshade of the HR-DSM of the Punta Cola rock avalanche scar and deposits. The TLS scan positions (yellow circles) and the cross-sections in Fig. 4 are shown.

spacing of 10.2 cm [min: 4.6 cm; max: 25.3 cm] at an average acquisition distance of 309 m [50 m; 880 m]. The total point cloud comprises 48.7 million points and covers a surface of approximately 1.4 km<sup>2</sup> (~35 points/m<sup>2</sup>).

The TLS datasets were treated and analysed using PolyWorks v11 software (InnovMetric 2011). The procedure includes a manual cleaning of the raw point clouds to remove unwanted objects, such as vegetation. The intact vegetation was kept in the scans, in order to easily map the run-up height of the rock avalanche. The cleaned scans are afterwards co-registered (or aligned) into a common reference system using first a manual matching and the identification of identical points in different scans, followed by an au-

tomatic iterative co-registration procedure, using an Iterative Closest Point algorithm (Besl and McKay 1992; Chen and Medioni 1992). Finally, the unified point cloud is georeferenced using the GPS coordinates of the 11 scanner locations. Details of the TLS data treatment procedure can be found in Oppikofer *et al.* (2009).

#### Geomorphologic mapping

A HR-DSM with a cell size of 25 cm was created from the TLS point cloud using Global Mapper v11 software (Global Mapper Software 2011). The HR-DSM was used in ArcGIS to create a hillshade (view-shaded relief representation) for the geomorphologic mapping, as well as the creation of contour lines (Fig. 3) and

cross-sections (Fig. 4). The geomorphologic mapping was performed at a scale of 1:1000 and focussed on rockslide scars (scarps, lateral release surfaces, sliding surface outcrops) and related deposits (limit of main and secondary deposits, limit of run-up) and was cross-validated by field observations, photographs and inspection of the TLS point cloud in PolyWorks.

#### Volume computation

In order to compute the volume of the Punta Cola rock avalanche and the secondary rockslides, as well as the deposited volumes, the pre-event topography needs to be reconstructed. This can be realized using aerial photographs (Mora *et al.* 2003; Dewitte *et al.* 2008; Prokesová

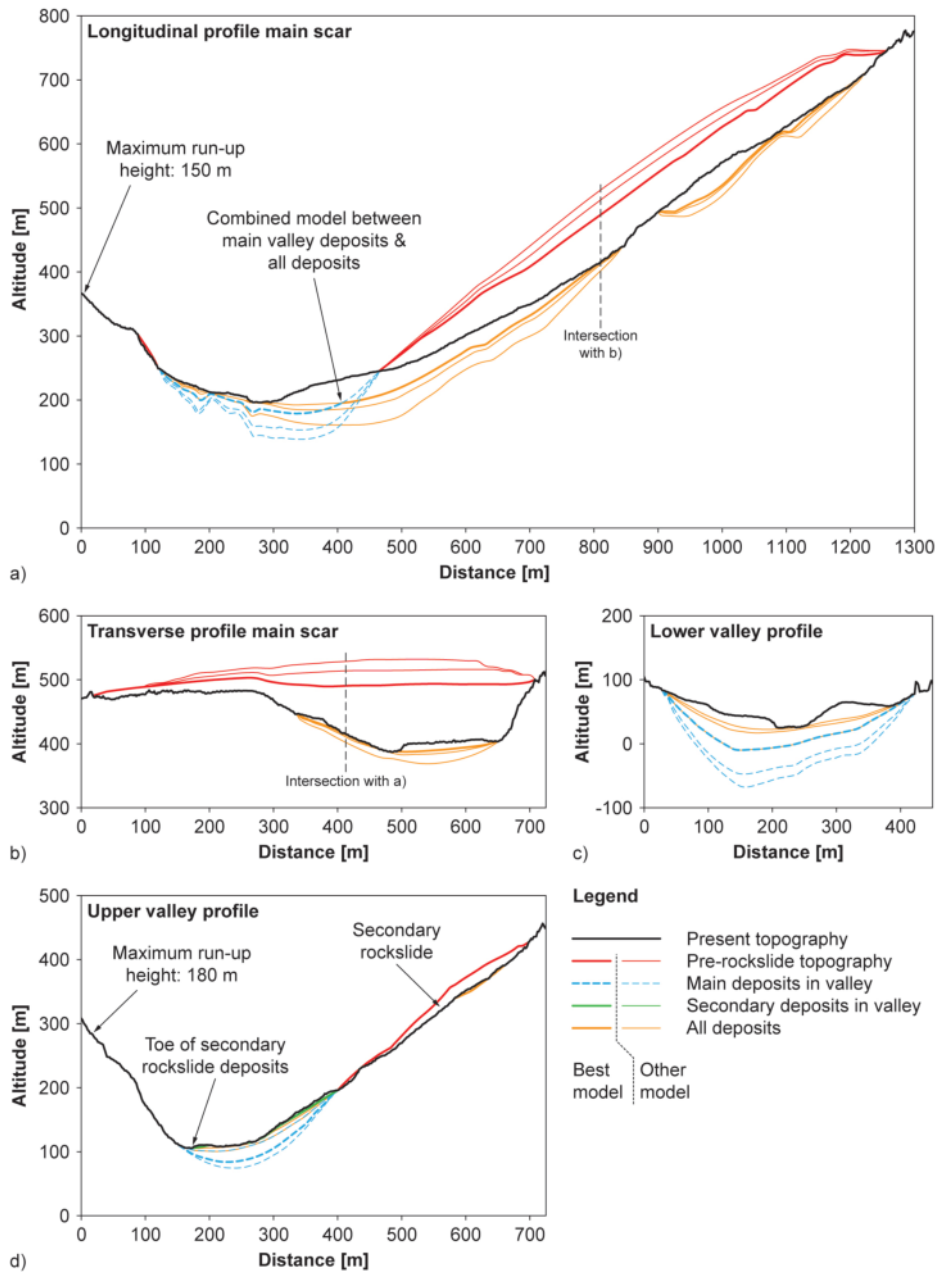


**Figure 4:** Cross-sections of the Punta Cola rock avalanche with different models for the pre-rockslide topography, the bedrock surface in the main valley and the rockslide scars: a) longitudinal profile across the main rockslide; b) transverse profile across the main rockslide; c) profile across the Punta Cola valley close to the shoreline; d) profile across the Punta Cola valley and a large secondary rockslide. See profile location in Fig. 3.

*et al.* 2010) or topographic maps (Evans *et al.* 2001) acquired before the event. Contour lines with an equidistance of 50 m of available 1:50'000 topographic maps (Instituto Geográfico Militar de Chile 1998a; Instituto Geográfico Militar de Chile 1998b) were used to create a pre-earthquake DEM with a cell size of 30 m. The poor horizontal and ver-

tical resolution of this DEM, however, impedes correct volume analyses of the rockslide and its deposits. Aerial photographs could provide a pre-earthquake DEM with better resolution (e.g. 5 m cell size), but will be affected by the dense vegetation cover of the Punta Cola valley. Other techniques focus on the surface reconstruction based on the continuity

between the present topography outside the scar area and the pre-event topography within the rockslide area. This can be achieved by following and completing the contour lines of the present-day topography over the rockslide scar (Brückl 2001) or by interpolation methods like inverse distance weighting (IDW) or kriging (Gorum *et al.* 2008). These latter techniques are however difficult to implement for volume of deposits estimations. The sloping local base level (SLBL) technique is an alternative interpolation technique and can be applied to create the pre-event topography in both rockslide scar and deposits area (Jaboyedoff *et al.* 2004; Jaboyedoff and Derron 2005; Travelletti *et al.* 2010). This technique has been developed to define a basal surface above which rock masses are prone to be eroded by mass wasting processes. This surface is computed by an iterative procedure, which flattens and lowers the spurs and spikes on the topography between user-defined fixed, invariant points (Jaboyedoff *et al.* 2004). The computed SLBL surface has a parabolic surface (second-order surface) with constant altitude tolerance  $\Delta z$ , which can be estimated using the valley width  $L$ , the assumed maximum deposits thickness  $h_{\max}$  (relative to a straight line between the limits) and the cell size  $\Delta x$  of the DEM or DSM (Jaboyedoff and Derron 2005):

$$\Delta z = \frac{4h_{\max}^2 \Delta x}{L^2}$$

The SLBL algorithm is used for four different models: 1) thickness of deposits in the main valley, 2) thickness of all deposits (main valley and rockslide scars), 3) the thickness of secondary rockslide deposits on the main rock avalanche deposits, and 4) reconstruction of the pre-event topography. The areas considered as variable in the SLBL computation for each model are shown in Table 1. Eight profiles across the valley and the main scar were created in order to measure the valley/scar width  $L$  and to estimate minimum, mean and maximum scenarios for the maximum thickness  $h_{\max}$  (see location in Fig. 3 and example profiles in Fig. 4). The resulting values for  $\Delta z$  for the different models are shown in Table 1.

**TABLE 1:** Minimum, mean and maximum altitude tolerances used for the SLBL computation of the deposits and pre-event topography of the Punta Cola rock avalanche.

Model	Variable areas (see Fig. 5)	Mean width L [m]	h max [m]			$\Delta z$ [m]		
			Min	Mean	Max	Min	Mean	Max
Deposits in main valley	Main and secondary deposits; River	244	24	37	45	0.00652	0.00994	0.01209
All deposits (valley & scars)	Main and secondary deposits; Rockslide scar with debris cover; River	655	83	108	175	0.00307	0.00402	0.00652
Secondary rockslide deposits	Secondary deposits	200	2	5	10	0.00080	0.00200	0.00400
Pre-event topography	Rockslide scar with outcrops; Rockslide scar with debris cover	626	11	19	27	0.00045	0.00078	0.00110

To compute the pre-event topography in the rockslide scar areas with the SLBL technique a trick is needed, because the SLBL algorithm is only able to lower the topography and not to raise it. By inverting the DEM (multiplying it by -1), crests become valleys and depressions become hills, which can be afterwards lowered with the SLBL algorithm (Oppikofer 2009). The volume contained between the modelled surfaces and the present topography is then calculated by summing the altitude differences over the considered area.

## RESULTS

### Morphology of rockslide scars

The main scar of the Punta Cola rock avalanche is nearly 1 km long and up to 760 m wide (Fig. 5). The height difference between the crown and the toe of the basal failure surface (BFS) is more than 530 m. The WNW-dipping BFS is exposed in the north-eastern part of the rockslide scar and displays a complex morphology using several pre-existing discontinuities, but also newly formed fractures (Fig. 2a). The rockslide scar is delimited to the south by an up to 115 m high WNW-ESE-trending lateral release surface (LRS) (Fig. 2a). Nearly 75% of the rockslide scar area is covered by debris, especially in the area between the exposed BFS and the LRS (Fig. 5). The HR-DSM reveals a clear break-line in the scar morphology above the exposed BFS at an altitude of ~550 m.a.s.l., which is marked by a lack of TLS data due to occlusions (Fig. 3, Fig. 4a). Redfield *et al.* (2011) have shown a highly fractured zone (maybe an active branch of

the LOFZ) crossing the rockslide scar just SE of the break-line in the topography.

A detailed structural analysis of the major discontinuities involved in the BFS and the LRS was made by Redfield *et al.* (2011) using the TLS point cloud in the software Coltop3D (Jaboyedoff *et al.* 2007; Terranum 2012). Seven distinct discontinuity sets were measured on the BFS. Five of them dip in W to NW direction with dip angles between 30° and 72°. Two other sets dip in SE to S direction with dip angles around 80° and form overhanging cliffs within the exposed BFS. The LRS also has a complex morphology and is shaped by a multitude of discontinuity sets. Subvertical north-dipping and south-dipping discontinuity sets define the main orientations of the LRS and its trace on the map (Fig. 5). These discontinuities accommodate mainly shear movements along the LRS, while NW-dipping discontinuities observed in the LRS are extensional structures (Redfield *et al.* 2011). Redfield *et al.* (2011) propose a wedge failure mechanism for the Punta Cola rockslide based on the observed structures. This wedge is formed by the intersection of a shallowly W-dipping discontinuity set (dip direction/dip angle: 283°/30° ± 8°) exposed in the BFS and a subvertical N-dipping discontinuity set (027°/80° ± 9°) observed in the LRS. Field observations show the existence of pre-existing brittle fault structures, in particular one low-angle thrust fault that is sub-parallel to the main basal sliding surface and that was possibly later reactivated under tensional conditions (Fig. 6a). Further field inspection shows the BFS to be characterized by

locally fairly planar surfaces with epidote and chlorite mineralization and down-dip to oblique mineral lineations preserved on many surfaces (Fig. 6b). However, there are no field evidences for low friction angles along the BFS, which would enable sliding on the shallowly-dipping BFS without seismic acceleration as triggering factor. This assumption needs further testing and validation, notably using numerical slope stability modelling.

Seven secondary rockslides occurred within the valley of the Punta Cola rock avalanche (Fig. 2b,d, Fig. 4d, Fig. 5). The largest of these secondary slides is located directly southwest of the main rockslide and has a very similar slope configuration (Fig. 2b). The scar is approximately 190 m wide and 280 m long. The altitude difference between head scarp and toe is about 215 m. The BFS is also dipping westwards and has a complex morphology formed by the intersection of multiple discontinuity sets. This lets suppose a similar failure mechanism and also a seismic acceleration as triggering factor. The other secondary slides are much smaller and – except one – are located on the SE-dipping valley site opposite to the main rockslide (Fig. 5).

### Morphology of deposits

The rock avalanche caused significant erosion along the 1.5 km long valley down to the Aysén fjord with a maximum run-up height of 150 m on the opposite valley flank (Fig. 4a). The limit of bare rock surfaces due to the stripping of soil and vegetation by the rock avalanche reaches even 180 m above the present valley floor (200 m above the modelled bedrock sur-

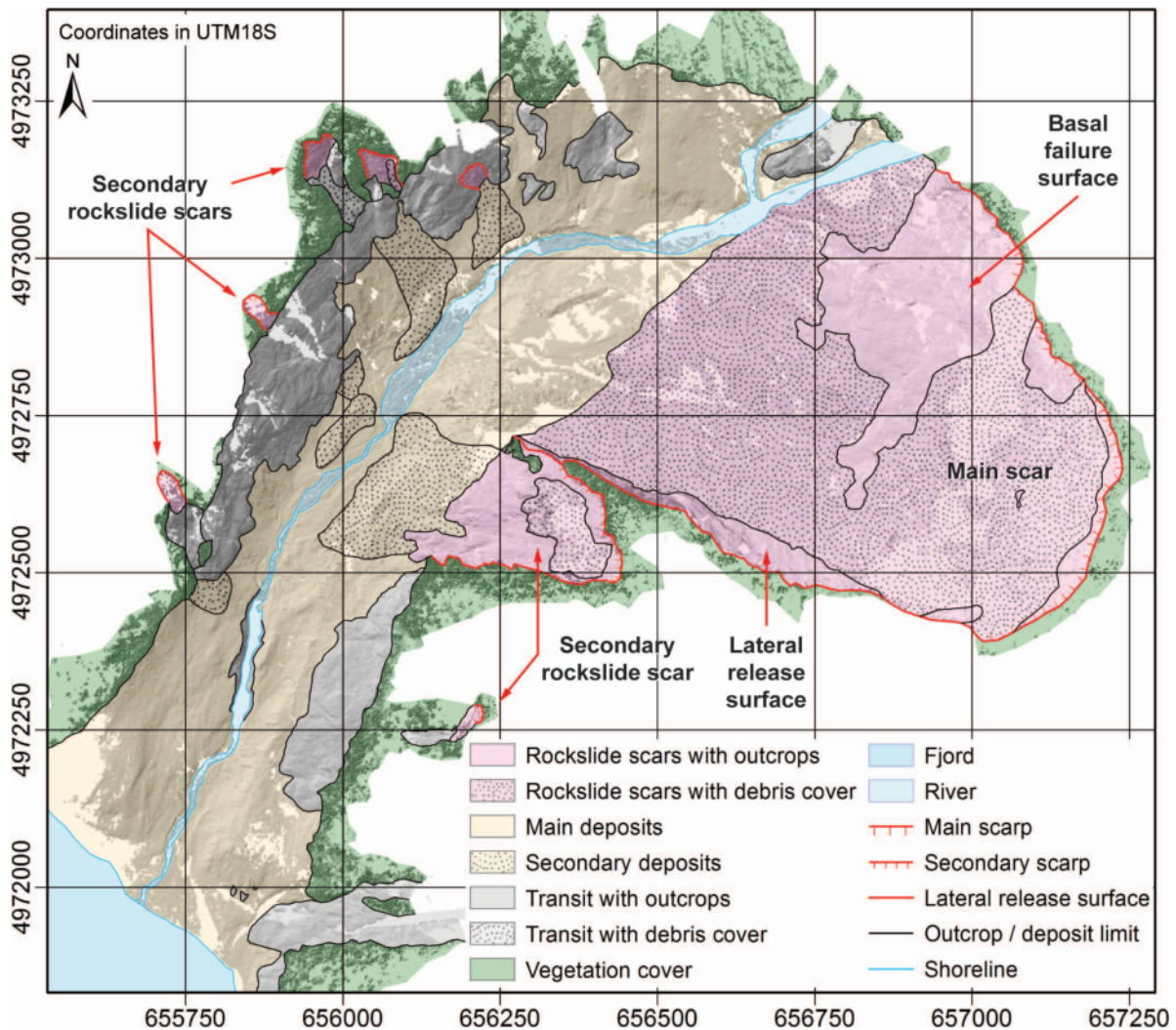


**Figure 5:** Geomorphologic map of the Punta Cola rock avalanche based on the HR-DSM and field observation.

face) at the location of the Upper valley profile in Fig. 4d. Bare rock surfaces are also mapped on the left valley side, which indicates that the rock avalanche also scoured these valley flanks (Fig. 5).

Close to the shoreline, rock avalanche deposits display a typical steep front that is more than 35 m high (Fig. 2c). The composition of the deposits varies between the two valley sides with more blocky material on the left valley side and more soil rich material on the right side. This higher soil content seems to be related to higher entrainment of soil and vegetation cover along the right valley flank compared to the left flank, where the rock avalanche run-up height was also lower. The detailed HR-DSM obtained by TLS

also allows understanding the sequence of sliding with the secondary rockslides having occurred after the main rock avalanche. Lobate landslide deposits with high soil content lie on top of fresh blocky rockslide debris (Fig. 2b-e). The largest of the secondary rockslides created a small rock avalanche that crossed the Punta Cola valley and likely blocked the river, which had to create a new path across these deposits. This is highlighted by the change of river bed width that passes from a 50 m wide, braided river above these secondary deposits to a 5 m wide torrent (Fig. 5).

The river path seems also to be modified at the foot of the main rockslide by thick, blocky rock avalanche deposits (Fig. 2a). On top of these deposits lie relatively in-

tact tree stems, indicating that the energy of the rock avalanche was not very high. This finding lets suppose that these deposits are created by the failure of a different compartment than the one that led to the main rock avalanche.

#### Volume of rockslides and deposits

The thickness of deposits in the Punta Cola valley and on the rockslide scars was estimated using different SLBL models with different scenarios (see Methods section, Table 1). The visual inspection of cross-sections (Fig. 4) allowed choosing the most plausible scenario to represent the bedrock surface under the rock avalanche deposits or the pre-rockslide topography. These most plausible scenarios can

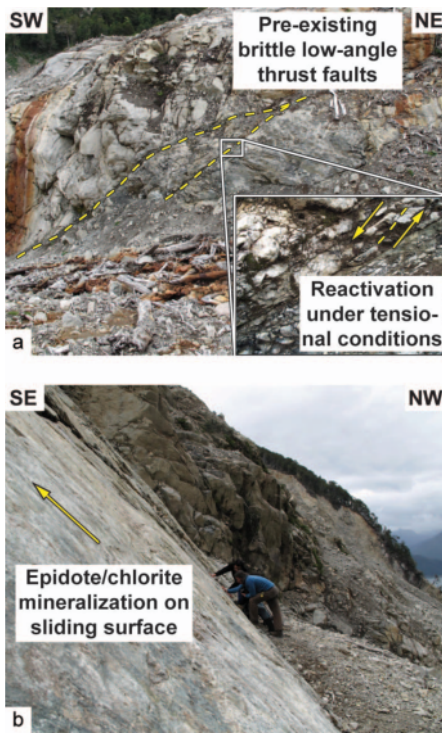


**Figure 6:** a) Photographs of pre-existing low-angle thrust faults that were reactivated under tensional conditions; b) Picture of the basal failure surface with an epidote/chlorite mineralization indicating thrust movement parallel to the thrust fault exposed in a).

be different from one cross-section to another, e.g. for the main deposits in the valley: minimum surface in the Longitudinal profile main scar (Fig. 4a) and the Lower valley profile (Fig. 4c); mean surface in the Upper valley profile (Fig. 4d). Finally, one scenario per model was chosen based on how often it was found to best represent the bedrock surface or the pre-rockslide topography (Table 2).

The SLBL model with all deposits (main valley and rockslide scars) leads to a con-

**TABLE 2:** Choice of one of three SLBL models (minimum, mean or maximum) based on visual inspection of cross-sections (see Fig. 4). The percentage indicates how often the given model was chosen to represent best the topography. Models with highest percentages are retained for the volume computation (grey-shaded).

Model	Min	Mean	Max
Deposits in main valley	63 %	38 %	0 %
All deposits (valley & scars)	67 %	24 %	10 %
Secondary rockslide deposits	20 %	0 %	80 %
Pre-event topography	64 %	31 %	6 %

ceivable estimation of the deposits thickness in the scar areas, but the computed thickness seems too low in the main valley (Fig. 4). On the contrary, the model for the main valley leads to a typical U-shaped valley that is more likely to match the bedrock surface. Therefore, the SLBL models were combined by using the maximum thickness of both models (see Fig. 4a). The final model of deposit thickness is shown in Fig. 7. Resulting volumes for the main deposits in the valley, the deposits of secondary rockslides and the deposits on the rockslide scars are also indicated in Fig. 7. The altitude differences between the modelled pre-rockslide topography and the present topography are shown in Fig. 8. For the volume of rockslides two variants are indicated in Fig. 8, one without and one with the deposits in the scar area. Including the deposits gives the total volume of the rockslide.

The main rockslide at Punta Cola had a volume of 22.4 Mm<sup>3</sup>, which includes about 4.0 Mm<sup>3</sup> of debris in the scar area. The average thickness is 52.2 m and reaches up to 111 m in the central part of the rockslide (Fig. 8, Table 3). The main deposits in the valley have a volume of 9.7 Mm<sup>3</sup> (mean thickness: 18.3 m; max. thickness: 82 m), which excludes the deposits of secondary rockslides lying on top. The total volume of onshore deposits of the main rock avalanche equals 13.7 Mm<sup>3</sup>. Assuming a typical bulking factor of 25% due to fragmentation (Hungur and Evans 2004) means that the volume deposited in the fjord should approximate 14.4 Mm<sup>3</sup>. The error on these volume estimations is difficult to quantify, but can be estimated using the different scenarios modelled by the SLBL. So, the errors are approximately 17% (3.8 Mm<sup>3</sup>) for the Punta Cola rockslide volume and 26% (3.5 Mm<sup>3</sup>) for the onshore deposits.

The SLBL model for the secondary deposits clearly underestimates their volume with respect to the modelled rockslide volumes (Fig. 7, Fig. 8). For example, the largest secondary rockslide has a total volume of 635'000 m<sup>3</sup> (after fragmentation: 790'000 m<sup>3</sup>), but the associated deposits in the valley and the scar equal only 251'000 m<sup>3</sup>. The other secondary

rockslides have relatively small volumes ranging from 3000 m<sup>3</sup> to 28'000 m<sup>3</sup> (Fig. 8). The associated deposits range from 600 m<sup>3</sup> to 47'000 m<sup>3</sup> (joint deposits from two rockslides) and are underestimated by a factor of 4 in average (Fig. 7). This shows one of the limitations of the SLBL approach, which is only able to simulate second order curved surfaces between the fixed points. Such a surface does not capture the likely interface between the main deposits or bedrock and the secondary deposits lying on top. Other techniques, for example the construction of the interface by planar surfaces in 3D, could overcome this limitation and provide more realistic results for the thickness and volume estimation of secondary deposits.

## INTERPRETATION

The 21 April 2007 Aysén earthquake triggered several rockslides in the Punta Cola valley. The geomorphologic mapping, the HR-DSM from TLS data and the volume computations indicate that the main rockslide likely occurred in several phases (Fig. 9). The south-western compartment (A in Fig. 9) is characterized by a high average rockslide thickness compared to the north-eastern compartment (B), which is relatively shallow (Table 3). The third compartment is formed by the south-eastern part of the rockslide scar above a break-line in the topography characterised by a highly fractured zone (C). The sequence of sliding of these compartments is difficult to elucidate and compartments A and B may have failed together or individually. Our current hypothesis is that compartment A was triggered by the main shocks of the 21 April 2007 Aysén earthquake and failed first (① in Fig. 9). This failure created a free face that allowed compartments B (①) and afterwards C to fail. The timing of these events can be very shortly after the main event.

The failed mass of compartment A (and maybe B) evolved as a rock avalanche with high-mobility with an angle of reach of approximately 15° (fall height: ~560 m; run-out length: >2000 m). The rock avalanche crossed the Punta Cola valley

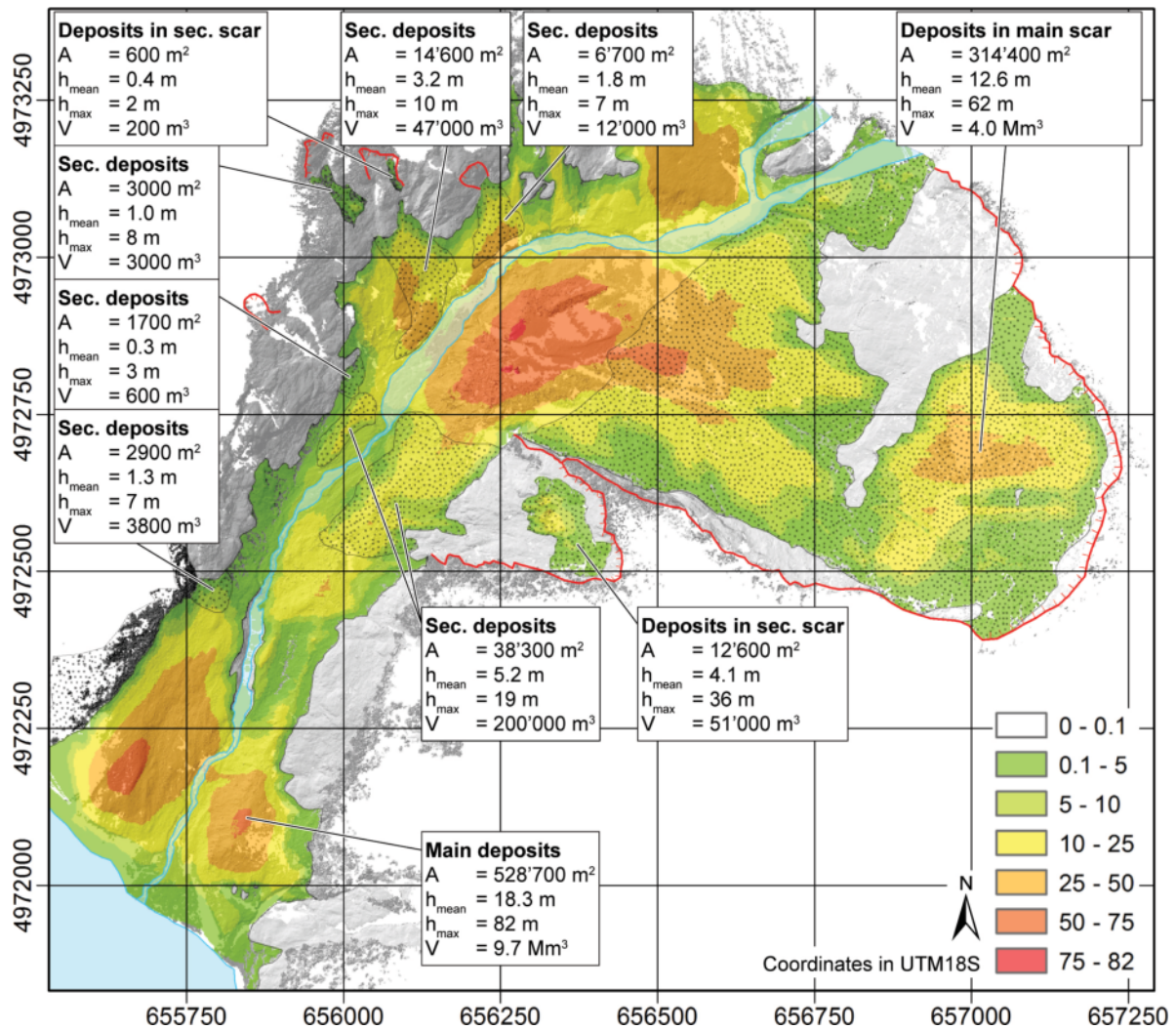


**Figure 7:** Deposits thickness of the Punta Cola rock avalanche based on the SLBL model. The total volume contained between the present surface and the modelled bedrock topography is shown.

and run up the opposite valley flank by up to 150 m (②). The rock avalanche stripped the soil and vegetation on the right valley side (③) before crossing the valley again and running up on the left valley side (④). A bedrock ridge located at about 400 m from the shoreline (⑤) was overrun by the rock avalanche. This ridge is covered by relatively thin deposits (Fig. 7), but probably reduced the mobility of the rock avalanche, which led to the deposition of more than 50 m thick debris close to the shoreline (⑥). Nonetheless the rock avalanche impacted the Aysén fjord and triggered a destructive tsunami (⑦).

In opposition to the rock avalanches created by the failure of compartments A

and B, the rock avalanche originating from compartment C had a lower mobility (angle of reach:  $\sim 27^\circ$ ). The rock avalanche stopped at the toe of the slope in the Punta Cola valley and led to thick debris deposits at the foot of the main rockslide scar (⑧, Fig. 7). The presence of

relatively intact tree stems on the top of these deposits (see Fig. 2a) are a further indication that the energy of the rock avalanche from compartment C was less important than the main rock avalanche. The other rockslides that were mapped in the Punta Cola valley (⑨, Fig. 5, Fig.

**TABLE 3:** Mean and maximum thickness between the modelled pre-event topography and the modelled bedrock surface and resulting volumes of different compartments of the main rockslide at Punta Cola.

Compartment	Area [m <sup>2</sup> ]	Mean thickness [m]	Max. thickness [m]	Volume [Mm <sup>3</sup> ]
A	205'500	71.7	111.0	14.7
B	104'000	23.8	55.7	2.5
C	120'000	43.3	107.1	5.2
Total	429'500	52.2	111.0	22.4

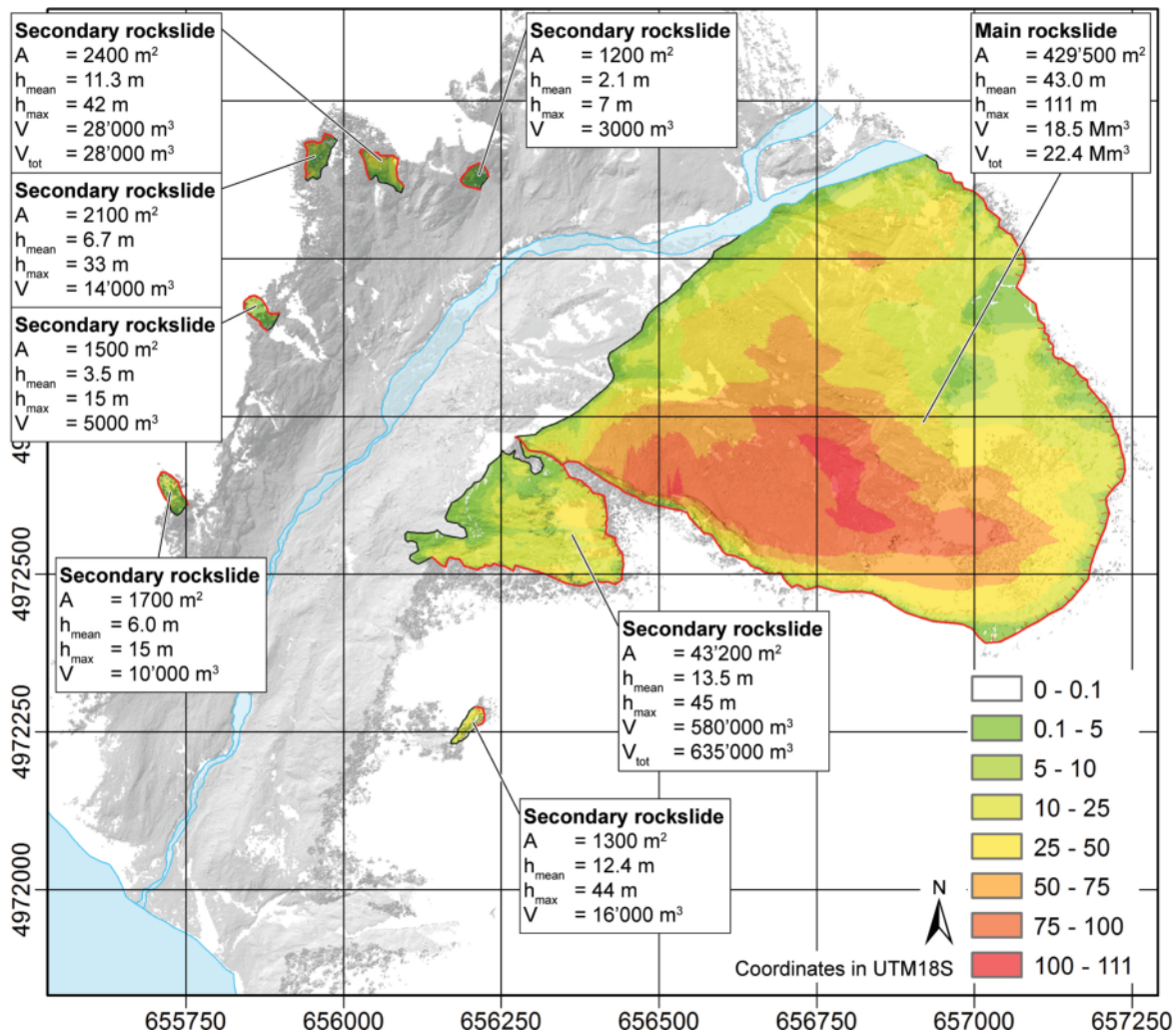


**Figure 8:** Altitude differences between the modelled pre-rockslide topography and the present surface. The volume of main and secondary rockslides is shown. The volume of a rockslide,  $V$ , can be increased by the volume of the deposits in the scar area (from Fig. 7) to obtain the total volume,  $V_{tot}$ .

9) have occurred after the main rock avalanche, since their deposits are found on top of the main deposits (10). These secondary rockslides were either triggered by earthquake aftershocks or by scouring of the valley flanks by the main rock avalanche.

## CONCLUSIONS

The study of the 2007 Punta Cola rock avalanche highlights the complex structures and mechanisms involved earthquake-triggered landslides with the simultaneous or quasi-simultaneous failure of several compartments that formed the main rock avalanche, but also of several secondary, minor rockslides.

The pre-existing discontinuity sets, especially the brittle fault planes, were important elements in the compartmentalization of the main Punta Cola rockslide by defining the location of the basal failure surface and by shaping its morphology. In particular, the basal failure plane is characterized by mineral lineations that bespeak of epidote-chlorite PT conditions, and is parallel to (and possibly coincident with) a well-developed low-angle fault with early compressive (thrust) and subsequent tensional kinematics. However, it remains open whether the slopes at Punta Cola would *a priori* have been recognised as unstable rock slopes that could fail under a seismic acceleration? Was there some pre-failure deformation,

such as long-term creep, or other signs of activity, such as frequent rockfalls and disrupted or disturbed vegetation, that could have been detected before the 2007 Aysén earthquake? These questions are crucial for the hazard assessment of rock slope instabilities and further investigations are necessary to answer them. A thorough analysis of historical aerial photographs will hopefully provide first indications.

The morphological analysis of the Punta Cola rock avalanche deposits shows also the complex propagation of the rock avalanche in the narrow valley with intense scouring along the valley flanks. Moreover, the rock avalanche likely occurred in several pulses with the main one reaching

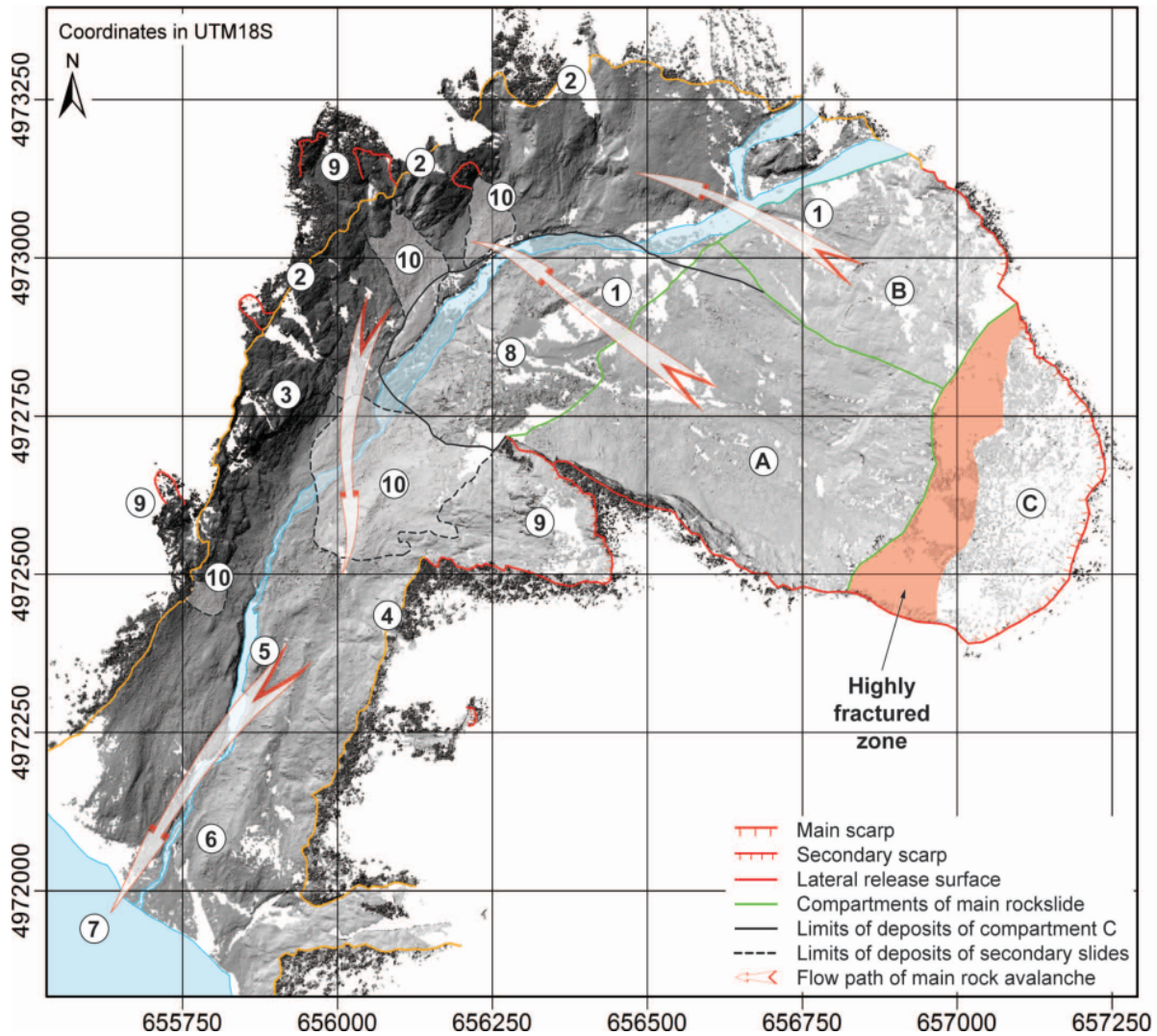


**Figure 9:** Interpretation of the sequence of sliding for the main and secondary rockslide at Punta Cola and their run-out. Letters A, B and C refer to different compartments of the main rockslide. Numbers indicate the sequence of events (see text for details).

the fjord and creating a tsunami, while the last one deposited its load at the toe of the main rockslide scar. To refine the proposed sequence of events, the pre-rockslide topography needs to be known more precisely, for example with the help of a digital elevation model produced from pre-event aerial photographs. Fjord bathymetry and seismic surveys are planned and will provide the morphology of the underwater deposits and enable the estimation of their volume. Combining these data with the high-resolution digital elevation model presented in this study will increase the understanding of the rock avalanche propagation and provide the

necessary input data for numerical rock avalanche propagation modelling.

This study highlights the additional information on rockslides and rock avalanches that are obtained from high-resolution digital elevation models created from aerial laser scanning or – as in this study – from terrestrial laser scanning point clouds. These precise and very dense 3D datasets open new ways of analysing the topography. The mapping of landslide and geomorphologic features is easier and more accurate using hillshades of digital elevation models in combination with field observations compared to field mapping.

#### ACKNOWLEDGEMENTS

This study was funded by the Research Council of Norway through the International Centre for Geohazards (ICG). Their support is gratefully acknowledged. This is ICG contribution 371. S. Sepúlveda acknowledges the Montessus de Ballore International Earthquake Research Center and Fondecyt project 11070107 for funding. The authors thank also their colleagues that participated in the field work. Andrés Folguera and Patricio Valderrama are kindly acknowledged for the review of the manuscript.

## LIST OF REFERENCES

- Abellán, A., Calvet, J., Vilaplana, J.M. and Blanchard, J. 2010. Detection and spatial prediction of rockfalls by means of terrestrial laser scanner monitoring. *Geomorphology* 119: 162-171. doi:10.1016/j.geomorph.2010.03.016.
- Abellán, A., Vilaplana, J.M. and Martínez, J. 2006. Application of a long-range terrestrial laser scanner to a detailed rockfall study at Vall de Núria (Eastern Pyrenees, Spain). *Engineering Geology* 88: 136-148. doi:10.1016/j.enggeo.2006.09.012.
- Alba, M., Longoni, L., Papini, M., Roncoroni, F. and Scaioni, M. 2005. Feasibility and problems of TLS in modeling rock faces for hazard mapping. *Proceedings of the ISPRS Workshop Laser scanning 2005, XXXVI, Part 3/W19*: 156-161, Enschede, the Netherlands.
- Baltsavias, E.P. 1999. Airborne laser scanning: Basic relations and formulas. *ISPRS Journal of Photogrammetry & Remote Sensing* 54: 199-214. doi:10.1016/S0924-2716(99)00015-5.
- Besl, P.J. and McKay, N.D. 1992. A method for registration of 3-D shapes. *IEEE Transactions on Pattern Analysis and Machine Intelligence* 14: 239-256.
- Bitelli, G., Dubbini, M. and Zanutta, A. 2004. Terrestrial laser scanning and digital photogrammetry techniques to monitor landslide bodies. *Proceedings of the XXth ISPRS Congress Geo-Imagery Bridging Continents, 35°, part B5*: 246-251, Istanbul, Turkey.
- Brückl, E.P. 2001. Cause-effect models of large landslides. *Natural Hazards* 23: 291-314.
- Cembrano, J., Hervé, F. and Lavenu, A. 1996. The Liquiñe Ofqui Fault Zone: A long-lived intra-arc fault system in southern Chile. *Tectonophysics* 259: 55-66.
- Cembrano, J., Lavenu, A., Reynolds, P., Arancibia, G., López, G. and Sanhueza, A. 2002. Late Cenozoic transpressional ductile deformation north of the Nazca-South America-Antarctica triple junction. *Tectonophysics* 354: 289-314.
- Chen, Y. and Medioni, G. 1992. Object modeling by registration of multiple range images. *IEEE International Conference on Robotics and Automation*: 2724-2729.
- Dewitte, O., Jasselette, J.C., Cornet, Y., Van Den Eeckhaut, M., Collignon, A., Poesen, J. and Demoulin, A. 2008. Tracking landslide displacements by multi-temporal DTMs: A combined aerial stereophotogrammetric and LIDAR approach in western Belgium. *Engineering Geology* 99: 11-22.
- Dunning, S.A., Massey, C.I. and Rosser, N.J. 2009. Structural and geomorphological features of landslides in the Bhutan Himalaya derived from terrestrial laser scanning. *Geomorphology* 103: 17-29. doi:10.1016/j.geomorph.2008.04.013.
- Evans, S.G. and Clague, J.J. 1994. Recent climatic change and catastrophic geomorphic processes in mountain environments. *Geomorphology* 10: 107-128.
- Evans, S.G., Hungr, O. and Clague, J.J. 2001. Dynamics of the 1984 rock avalanche and associated distal debris flow on Mount Cayley, British Columbia, Canada; implications for landslide hazard assessment on dissected volcanoes. *Engineering Geology* 61: 29-51.
- Fardin, N., Stephansson, O. and Jing, L. 2001. The scale dependence of rock joint surface roughness. *International Journal of Rock Mechanics and Mining Sciences* 38: 659-669. doi:10.1016/S1365-1609(01)00028-4.
- Folguera, A., Ramos, V.A., Hermanns, R.L. and Naranjo, J.A. 2004. Neotectonics in the foothills of the southernmost central Andes (37°-38°S): Evidence of strike-slip displacement along the Antifñir-Copahue fault zone. *Tectonics* 23: TC5008. doi:10.1029/2003TC001533.
- Global Mapper Software, 2011. GIS Mapping Software - GPS Mapping Software - Satellite Maps - Aerial Photos [Global Mapper]. <http://globalmapper.com>, accessed 02.03.2012.
- Gorum, T., Gonencgil, B., Gokceoglu, C. and Nefeslioglu, H.A. 2008. Implementation of reconstructed geomorphologic units in landslide susceptibility mapping: The Melen gorge (NW Turkey). *Natural Hazards* 46: 323-351. doi:10.1007/s11069-007-9190-6.
- Hermanns, R.L., Fauque, L., Small, L.F., Welkner, D., Folguera, A., Cazas, A. and Nuñez, H. 2008. Overview of Catastrophic Megarockslides in the Andes of Argentina, Bolivia, Chile, Ecuador and Peru. *Proceedings of the First World Landslide Forum*: 255-258.
- Hermanns, R.L., Folguera, A., Penna, I.M., Fauque, L. and Niedermann, S. 2011. Landslide dams in the Central Andes of Argentine (Northern Patagonia and the Argentine Northwest). In Evans, S.G., Hermanns, R.L., Strom, A. and Scarascia Mugnozza, G. (eds.) *Natural and artificial rockslide dams*, Springer: 147-176, Berlin, Germany.
- Hungr, O. and Evans, S.G. 2004. Entrainment of debris in rock avalanches: An analysis of a long run-out mechanism. *Geological Society of America Bulletin* 116: 1240-1252. doi:10.1130/B25362.1.
- InnovMetric 2011. PolyWorks: 3D scanner and 3D digitizer software from InnovMetric Software Inc. <http://www.innovmetric.com/polyworks/3D-scanners/home.aspx?lang=en>, accessed 20.01.2012.
- Instituto Geográfico Militar de Chile 1998a. Fiordo Aisen. 1:50000: I-105.
- Instituto Geográfico Militar de Chile 1998b. Puerto Aisen. 1:50000: I-106.
- Jaboyedoff, M. and Derron, M.-H. 2005. A new method to estimate the infilling of alluvial sediment of glacial valleys using a sloping local base level. *Geografica Fisica e Dinamica Quaternaria* 28: 37-46.
- Jaboyedoff, M., Baillifard, F., Couture, R., Locat, J. and Locat, P. 2004. Toward preliminary hazard assessment using DEM topographic analysis and simple mechanical modeling by means of sloping local base level. In Lacerda, W.A., Ehrlich, M., Fontoura, A.B. and Sayão, A. (eds.) *Landslides: Evaluation and Stabilization*, Taylor & Francis Group: 199-205, London.
- Jaboyedoff, M., Metzger, R., Oppikofer, T., Couture, R., Derron, M.-H., Locat, J. and Turmel, D. 2007. New insight techniques to analyze rock-slope relief using DEM and 3D-imaging cloud points: COLTOP-3D software. In Eberhardt, E., Stead, D. and Morrison, T. (eds.) *Rock mechanics: Meeting Society's challenges and demands*. *Proceedings of the 1st Canada - U.S. Rock Mechanics Symposium, Vancouver, Canada, 27-31 May 2007*, Taylor & Francis: 61-68, London.
- Jaboyedoff, M., Demers, D., Locat, J., Locat, A., Locat, P., Oppikofer, T., Robitaille, D. and Turmel, D. 2009a. Use of terrestrial

- laser scanning for the characterization of retrogressive landslides in sensitive clay and rotational landslides in river banks. *Canadian Geotechnical Journal* 46: 1379-1390. doi:10.1139/T09-073.
- Jaboyedoff, M., Pedrazzini, A., Loye, A., Oppikofer, T. and Güell i Pons, M. 2009b. Earth flow in a complex geological environment: the example of Pont Bourquin, Les Diablerets (Western Switzerland). *Landslides Processes – From Geomorphologic mapping to dynamic modeling*, Proceedings of the landslide processes conference: 131-137.
- Jaboyedoff, M., Oppikofer, T., Abellán, A., Deron, M.-H., Loye, A., Metzger, R. and Pedrazzini, A. 2012. Use of LIDAR in landslide investigations: A review. *Natural Hazards* 61: 5-28. doi:10.1007/s11069-010-9634-2.
- Kemeny, J., Turner, K. and Norton, B. 2006. LIDAR for rock mass characterization: hardware, software, accuracy and best-practices. In Tonon, F. and Kottenstette, J. (eds.) *Laser and Photogrammetric Methods for Rock Face Characterization*, ARMA: 49-62.
- Kulatilake, P., Balasingam, P., Park, J. and Morgan, R. 2006. Natural rock joint roughness quantification through fractal techniques. *Geotechnical and Geological Engineering* 24: 1181-1202. doi:10.1007/s10706-005-1219-6.
- Lato, M., Diederichs, M.S., Hutchinson, D.J. and Harrap, R. 2009. Optimization of LIDAR scanning and processing for automated structural evaluation of discontinuities in rockmasses. *International Journal of Rock Mechanics and Mining Sciences* 46: 194-199. doi:10.1016/j.ijrmms.2008.04.007.
- Lavenu, A. and Cembrano, J. 1999. Compressional- and transpressional-stress pattern for Pliocene and Quaternary brittle deformation in fore arc and intra-arc zones (Andes of Central and Southern Chile). *Journal of Structural Geology* 21: 1669-1691. doi:10.1016/S0191-8141(99)00111-X.
- Legrand, D., Barrientos, S., Bataille, K., Cembrano, J. and Pavez, A. 2011. The fluid-driven tectonic swarm of Aysén Fjord, Chile (2007) associated with two earthquakes ( $M_w = 6.1$  and  $M_w = 6.2$ ) within the Liquiñe-Ofqui Fault Zone. *Continental Shelf Research* 31: 154-161. doi: 10.1016/j.csr.2010.05.008.
- Lichti, D.D., Gordon, S.J. and Stewart, M.P. 2002. Ground-based laser scanners: Operation, systems and applications. *Geomatica* 56: 21-33.
- Mora, P., Baldi, P., Casula, G., Fabris, M., Ghirrotti, M., Mazzini, E. and Pesci, A. 2003. Global positioning systems and digital photogrammetry for the monitoring of mass movements: Application to the Ca'di Malta landslide (Northern Apennines, Italy). *Engineering Geology* 68: 103-121.
- Naranjo, J.A., Arenas, M., Clavero, J. and Muñoz, O. 2009. Mass movement-induced tsunamis: Main effects during the Patagonian fjordland seismic crisis in Aisén ( $45^{\circ}25'S$ ), Chile. *Andean Geology* 36: 137-145.
- Nguyen, H.T., Fernandez-Steeger, T.M., Wiatir, T., Rodrigues, D. and Azzam, R. 2011. Use of terrestrial laser scanning for engineering geological applications on volcanic rock slopes - an example from Madeira Island (Portugal). *Natural Hazards and Earth System Sciences* 11: 807-817. doi:10.5194/nhess-11-807-2011.
- Oppikofer, T. 2009. Detection, analysis and monitoring of slope movements by high-resolution digital elevation models. PhD thesis, Institute of Geomatics and Analysis of Risk, University of Lausanne, Lausanne, Switzerland.
- Oppikofer, T., Jaboyedoff, M. and Keusen, H.-R. 2008. Collapse at the eastern Eiger flank in the Swiss Alps. *Nature Geoscience* 1: 531-535. doi:10.1038/ngeo258.
- Oppikofer, T., Jaboyedoff, M., Blikra, L.H. and Derron, M.-H. 2009. Characterization and monitoring of the Åknes rockslide using terrestrial laser scanning. *Natural Hazards and Earth System Sciences* 9: 1003-1019. doi:10.5194/nhess-9-1003-2009.
- Oppikofer, T., Jaboyedoff, M., Pedrazzini, A., Derron, M.-H. and Blikra, L.H. 2011. Detailed DEM analysis of a rockslide scar to improve the basal failure surface model of active rockslides. *Journal of Geophysical Research*. 116: F02016. doi:10.1029/2010JF001807.
- Optech 2011. ILRIS-3D Intelligent Laser Ranging and Imaging System. <http://optech.ca/i3dprodline-ilris3d.htm>, accessed 20.01.2012.
- Pankhurst, R.J., Weaver, S.D., Hervé, F. and Larrondo, P. 1999. Mesozoic-Cenozoic evolution of the North Patagonian Batholith in Aysén, southern Chile. *Journal of the Geological Society* 156: 673-694.
- Pedrazzini, A., Oppikofer, T., Jaboyedoff, M., Guell i Pons, M., Chantry, R. and Stampfli, E. 2010. Assessment of rockslide and rockfall problems in an active quarry: case study of the Arvel quarry (Western Switzerland). *Rock Mechanics in Civil and Environmental Engineering*: 593-596.
- Penna, I.M., Hermanns, R.L., Niedermann, S. and Folguera, A. 2011. Multiple slope failures associated with neotectonic activity in the southern central Andes ( $37^{\circ}$ - $37^{\circ}30'S$ ), Patagonia, Argentina. *Geological Society of America Bulletin* 123: 1880-1895. doi:10.1130/B30399.1.
- Prokesová, R., Kardos, M. and Medvedová, A. 2010. Landslide dynamics from high-resolution aerial photographs: A case study from the western Carpathians, Slovakia. *Geomorphology* 115: 90-101. doi:10.1016/j.geomorph.2009.09.033.
- Redfield, T.F., Hermanns, R.L., Oppikofer, T., Duhart, P., Mella, M., Derch, P., Basuñán, I., Arenas, M., Fernandez, J., Sepúlveda, S.A., Rebolledo, S., Loew, S., Yugsi Molina, F.X., Abärcherli, A., Henderson, I.H.C., Jaboyedoff, M. and Kveldevik, V. 2011. Analysis of the 2007 earthquake-induced Punta Cola rockslide and tsunami, Aysén Fjord, Patagonia, Chile ( $45.3^{\circ}$  S,  $73.0^{\circ}$  W). 5th International Conference on Earthquake Geotechnical Engineering.
- Rosser, N.J., Petley, D.N., Lim, M., Dunning, S.A. and Allison, R.J. 2005. Terrestrial laser scanning for monitoring the process of hard rock coastal cliff erosion. *Quarterly Journal of Engineering Geology and Hydrogeology* 38: 363-375. doi:10.1144/1470-9236/05-008.
- Rowlands, K.A., Jones, L.D. and Whitworth, M. 2003. Landslide laser scanning: A new look at an old problem. *Quarterly Journal of Engineering Geology and Hydrogeology* 36: 155-157.
- Sepúlveda, S.A. and Serey, A. 2009. Tsunami-genic, earthquake-triggered rock slope failures during the April 21, 2007 Aisén earthquake, southern Chile ( $45.5^{\circ}$ S). *Andean*

- Geology 36: 131-136. doi:10.4067/S0718-71062009000100010.
- Sepúlveda, S.A., Serey, A., Lara, M., Pavez, A. and Rebolledo, S. 2010. Landslides induced by the April 2007 Aysén fjord earthquake, Chilean Patagonia. *Landslides* 7: 483-492. doi:10.1007/s10346-010-0203-2.
- Sturzenegger, M. and Stead, D. 2009a. Close-range terrestrial digital photogrammetry and terrestrial laser scanning for discontinuity characterization on rock cuts. *Engineering Geology*. 106: 163-182. doi:10.1016/j.eng-geo.2009.03.004.
- Sturzenegger, M. and Stead, D. 2009b. Quantifying discontinuity orientation and persistence on high mountain rock slopes and large landslides using terrestrial remote sensing techniques. *Natural Hazards and Earth System Sciences*. 9: 267-287. doi:10.5194/nhess-9-267-2009.
- Terranum, 2012. Terr@num – Geoscience and software solutions. <http://www.terranum.ch/coltop3d-features>, accessed 20.01.2012.
- Teza, G., Galgaro, A., Zaltron, N. and Genevois, R. 2007. Terrestrial laser scanner to detect landslide displacement fields: A new approach. *International Journal of Remote Sensing* 28: 3425-3446.
- Travelletti, J., Demand, J., Jaboyedoff, M. and Marillier, F. 2010. Mass movement characterization using a reflexion and refraction seismic survey with the sloping local base level concept. *Geomorphology* 116: 1-10. doi:10.1016/j.geomorph.2009.10.006.

Recibido: 11 de febrero, 2012  
Aceptado: 23 de abril, 2012